Journal of Structural Biology: X 9 (2024) 100101

Contents lists available at ScienceDirect

Journal of Structural Biology: X

journal homepage: www.sciencedirect.com/journal/journal-of-structural-biology-x

Research Article

Coordination of bilayer properties by an inward-rectifier K^+ channel is a cooperative process driven by protein-lipid interaction

Evan J. van Aalst [a], Maryam Yekefallah [a], Roy A. M. van Beekveld [b], Eefjan Breukink [c], Markus Weingarth [b], Benjamin J. Wylie [a,*]

[a] Department of Chemistry and Biochemistry, Texas Tech University, Lubbock, TX 79409, USA
[b] Department of Chemistry, Faculty of Science, Utrecht University, Padualaan 8, 3584 CH, Utrecht, the Netherlands
[c] Membrane Biochemistry and Biophysics, Department of Chemistry, Utrecht University, Padualaan 8, 3584 CH, Utrecht, the Netherlands

ARTICLE INFO

Keywords:
SSNMR
Kir Channel
KirBac1.1
Phase Transition
Lipid Allostery
Cooperativity

ABSTRACT

Physical properties of biological membranes directly or indirectly govern biological processes. Yet, the interplay between membrane and integral membrane proteins is difficult to assess due to reciprocal effects between membrane proteins, individual lipids, and membrane architecture. Using solid-state NMR (SSNMR) we previously showed that KirBac1.1, a bacterial Inward-Rectifier K^+ channel, nucleates bilayer ordering and microdomain formation through tethering anionic lipids. Conversely, these lipids cooperatively bind cationic residues to activate the channel and initiate K^+ flux. The mechanistic details governing the relationship between cooperative lipid loading and bilayer ordering are, however, unknown. To investigate, we generated KirBac1.1 samples with different concentrations of ^{13}C-labeled phosphatidyl glycerol (PG) lipids and acquired a full suite of SSNMR 1D temperature series experiments using the ordered all-trans (AT) and disordered *trans*-gauche (TG) acyl conformations as markers of bilayer dynamics. We observed increased AT ordered signal, decreased TG disordered signal, and increased bilayer melting temperature with increased PG concentration. Further, we identified cooperativity between ordering and direct binding of PG lipids, indicating KirBac1.1-driven bilayer ordering and microdomain formation is a classically cooperative Hill-type process driven by and predicated upon direct binding of PG lipids. Our results provide unique mechanistic insight into how proteins and lipids in tandem contribute to supramolecular bilayer heterogeneity in the lipid membrane.

Introduction

Regulation of membrane protein structure and function by the lipid environment is ubiquitous. Cholesterol (van Aalst and Wylie, 2021; Calmet et al., 2020; Baccouch et al., 2022; Ray et al., 2023) and phosphatidylinositol-4,5-bisphosphate (PIP_2) (D'Avanzo et al., 2010; Xie et al., 2008; Thakur et al., 2023) are common allosteric lipids in eukaryotes while in prokaryotes, pentacyclic hopanoids (Sefah and Mertz, 2021; Belin et al., 2018) and anionic phospholipids like phosphatidyl glycerol (PG) (Laganowsky et al., 2014) and Cardiolipin (CL) (Patrick et al., 2018) serve similar purposes. Yet, as the bilayer influences protein structure and function, so too does the protein impart physical changes to the membrane environment. In bilayer systems, this may manifest as alterations and broadening of the temperature range in which the bilayer phase transitions from the gel phase (L_β) to liquid crystalline (L_α) phase, as well as partitioning of the liquid crystalline phase into liquid ordered (L_o) and liquid disordered (L_d) domains (Brown and London, 1998; Brown and London, 1998; Morvan et al., 2023; Mitchison-Field and Belin, 2023). Such interactions are inherently difficult to fully capture, thus the entire system must be considered since lipids as allosteric effectors do not exist in a vacuum. Solid-state Nuclear Magnetic Resonance (SSNMR) is an excellent technique to probe bilayer phase dynamics (Morvan et al., 2023; Vist and Davis, 1990; Kwon et al., 2013; Warnet et al., 2016; Morvan et al., 2023; Borcik et al., 2022; Della Ripa et al., 2023) and the intricacies of protein-lipid association, including G protein-Coupled Receptors (GPCRs) (Ahuja et al., 2009; Kimata et al., 2016; Kimata et al., 2016; Mertz et al., 2012; van Aalst et al., 2023; Becker-Baldus et al., 2023) and ion channels (Borcik et al., 2022; Borcik et al., 2020). Therefore, it is a powerful tool to gauge protein-lipid reciprocity in the context of protein-dependent tuning of bilayer structural architecture.

Inward-rectifier K^+ (Kir) channels are tetrameric integral membrane

* Corresponding author.
E-mail address: Benjamin.j.wylie@ttu.edu (B.J. Wylie).

https://doi.org/10.1016/j.yjsbx.2024.100101
Received 19 March 2024; Accepted 27 May 2024
Available online 28 May 2024

proteins which preferentially conduct K^+ into the cell (Lopatin et al., 1994; Hibino et al., 2010). Both prokaryotic and eukaryotic Kir channels share a common activation motif, where anionic phospholipids directly bind to a highly cationic lipid-binding domain at the intracellular water–lipid interface to induce channel activation (Hansen et al., 2011; Whorton and MacKinnon, 2011; Clarke et al., 2010; Huang et al., 1998; Soom et al., 2001; Meng et al., 2012). KirBac1.1 is a bacterial Kir channel (Cheng et al., 2009; Matamoros and Nichols, 2021) activated by PG and CL, which bind to this concerted Arg and Lys-rich pocket (Fig. 1A-B) (Borcik et al., 2020). This pocket also contains well conserved Tryptophan residues previously observed to be involved in lipid binding, though their role is not well understood (Borcik et al., 2022; Yekefallah et al., 2024). The binding event is translated through the transmembrane allosteric network to the selectivity filter and the helical bundle crossing, ultimately leading to channel activation (Amani et al., 2020). KirBac1.1 also nucleates bilayer ordering in simple synthetic mixtures (Amani et al., 2020) and complex biological extracts (Borcik et al., 2019), which manifests as a broadened phase transition range and enhanced L_o domain formation. When R49, R151, R153, and R181 are mutated to glutamine, channel activity is greatly reduced (Yekefallah et al., 2022). Curiously, these mutations also coincide with severely attenuated lipid ordering, indicating the ordering effect and lipid interaction are strongly entwined (Amani et al., 2020).

Previously, we used ^{13}C-labeled PG lipids extracted from *Staphylococcus simulans* to directly characterize PG affinity for KirBac1.1 using SSNMR (Yekefallah et al., 2024). In that work, chemical shift perturbations (CSPs) in the headgroup region corresponding to bound PG lipids were identified in 2D homonuclear correlation spectra and 1D Direct Polarization (DP) experiments. When the peak volume of the bound peak from DP spectra was plotted as a function of PG mol% (X_{PG}) in the bilayer, a sigmoidal curve was observed. So-called 'S' shaped curves are indicative of classical cooperativity in biological systems, which is defined by the Hill-Langmuir equation (Hill, 1913; Hill, 1909; Langmuir, 1918):

$$\theta = \frac{[L]^n}{[L]^n + K_d} \quad (1)$$

Here, ligand occupancy (θ) is a function of ligand affinity (dissociation constant, K_d) and cooperativity (Hill coefficient, n) when the ligand L is titrated. Using this equation, a PG-KirBac1.1 K_d of ~ 7 % X_{PG} was extrapolated. The results of this study indicated classic Hill-type cooperativity between subunits, where interaction of one subunit with PG lipids positively influences the kinetics of lipid interaction with neighboring subunits. While this work primarily focused on the protein, the pattern of changing linewidths with increased temperature was qualitatively observed to change with changing bilayer PG content.

To further investigate this result, we acquired full suites of 1D temperature series DP experiments and used the spectroscopically distinct (Purusottam et al., 2015) all-trans (AT, ~35 ppm) and *trans*-gauche (TG, ~33 ppm) acyl chain conformations as markers of bilayer ordering and melting, respectively. Since bilayer melting is inherently a cooperative process (Schneider et al., 1999), we sought to understand the reciprocity between lipid dynamics, bilayer melting, and lateral domain formation as a function of protein-lipid interactions. We observed that increasing PG in the presence of KirBac1.1 was positively correlated to increased bilayer ordering in the form of a broadened phase transition range centered at increasingly higher temperatures. This was observed despite the lipids available being predominately methylated, which negatively influences the efficacy of acyl packing (Hirata and Axelrod, 1980). We plotted DP peak volume corresponding to the AT peak and identified cooperative evolution of ordered lipids with PG concentration. Interestingly, when plotted against the previously identified bound PG lipid signal, we again observed cooperativity, indicating a positive correlation between KirBac1.1 binding PG, and PG lipids in turn presenting in the ordered, AT acyl conformation. To emphasize this point, we acquired refocused Insensitive Nuclei Enhance by Polarization Transfer (rINEPT) (Elena et al., 2005) spectra in temperature series and plotted TG melting curves as a function of PG concentration. We observed the melting temperature (T_m) cooperatively increased with PG concentration until ~ 10 % X_{PG}, where KirBac1.1 is expected to be saturated with PG, before sharply retracing. This result further suggests the ordering effect is predicated upon anionic lipid binding. To belabor this point, we plotted TG peak volume against PG concentration and bound peak volume from DP spectra and identified negative cooperativity in both cases. In concert, our results indicate that KirBac1.1 nucleates bilayer through direct lipid-protein interactions, and the cooperative nature of the binding event is translated to cooperative coordination of bilayer properties. This report highlights the functional interplay between membrane proteins and lipid-binding that directly shapes the dynamics of membrane structural architecture.

Material and Methods

Expression and Purification of Biological Macromolecules.

^{13}C-labeled PG lipids were purified as previously described

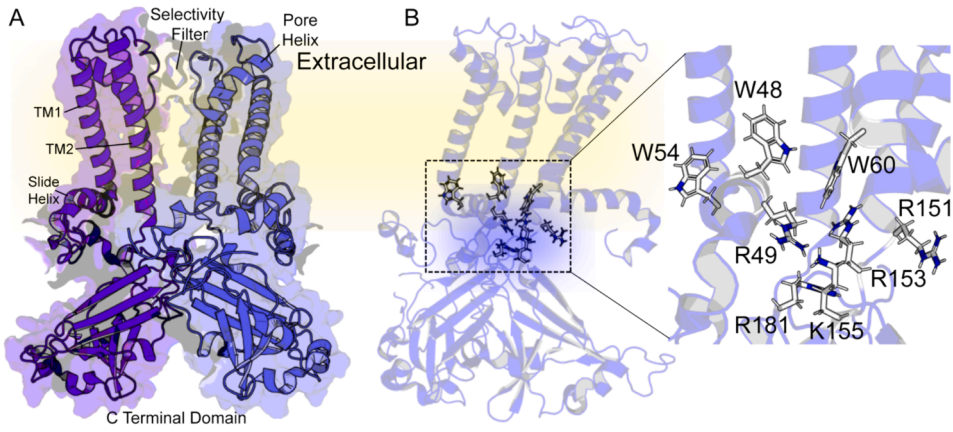

Fig. 1. KirBac1.1 is an inward rectifier K^+ channel that is activated by anionic phospholipids. (A) NMR-refined structure of KirBac1.1 (PDB 7SWJ) (Amani et al., 2021). The structure is presented as a cutaway with opposing subunits colored blue and purple. Structural motifs of interest are labeled. (B) The lipid-binding pocket is highlighted, shown on adjacent subunits of KirBac1.1. Cationic and hydrophobic lipid-interacting residues W48, R49, W54, and W60 in the slide helix and R151, R153, K155, and R181 in the neighboring subunit comprising the pocket are labeled. The approximate positioning of the membrane is shown in yellow, highlighting optimal positioning at the water–lipid interface to interact with lipid headgroups. (For interpretation of the references to colour in this figure legend, the reader is referred to the web version of this article.)

(Yekefallah et al., 2024; van Beekveld et al., 2022). Briefly, *S. simulans* cultures were grown for ~ 16 h at 37 °C and 220 RPM in Luria broth (LB) prior to resuspension in isotpocially enriched expression media (60 v/v % ^{13}C,^{15}N Silantes OD2 (Cambridge Isotopes), 0.5 v/v% ^{13}C,^{15}N Bio-Express (Cambridge Isotopes), 2 g/L U-^{13}C-D-Glucose, 1 g/L U-$^{15}NH_4Cl$, 6 g/L Na_2HPO_4, 3 g/L KH_2PO_4, and 0.5 g/L NaCl). Pellets were harvested after ~ 6 h, at an $OD_{600} = 4.5$ and treated with lysozyme for 2 h prior to total lipid extraction following the Bligh-Dyer method (Bligh and Dyer, 1959). The resulting film was resuspended in $CHCl_3$, loaded onto a silica column, and PG was eluted via isocratic elution with 48:48:3:1 $CHCl_3$:EtOH:H_2O:NH_3.

Expression and purification of KirBac1.1 was performed as previously described (Borcik et al., 2022; Borcik et al., 2020; Amani et al., 2021; Amani et al., 2020; Borcik et al., 2019; Yekefallah et al., 2022). Briefly, expression of natural abundance (NA) KirBac1.1 I131C stability mutant (SM) (Wang et al., 2009) was induced with 1 mM isopropyl *β*-D-1-thiogalactopyranoside (IPTG) at an $OD_{600} = 0.9–1.0$ in Terrific Broth (TB) for ~ 18 h at 18 °C, 220 RPM. Cell pellets were resuspended in lysis buffer at 5 mL/g cells (50 mM Tris-Base pH 8, 150 mM KCl, 250 mM Sucrose,10 mM $MgSO_4$, 1 mM benzamidine, 1 mM phenylmethylsulfonyl fluoride, 0.2 mg/mL lysozyme, 0.2 mg/mL RNAse, protease inhibitor tablets). Cells were homogenized to induce lysis and KirBac1.1 was extracted from membrane fragments with 30 mM decyl-β-D-maltopyranoside (DM) for 3–4 h at 4 °C with rocking. Debris was centrifuged at 125,000 g for 1 h, sterile filtered, and KirBac1.1 was separated from the lysate using a Ni^{2+} affinity column (HisTrap™, Cytiva) and Elution buffer (50 mM Tris-Base pH 8, 150 mM KCl, 5 mM dodecyl-β-D-maltopyranoside (DDM), 250 mM Imidazole). Imidazole was removed using a Desalting column (Cytiva), then KirBac1.1 was concentrated to ~ 2 mg/mL using a 100 kDa cutoff membrane filter (Millipore), loaded onto a 16/600 prep-grade 200 Size Exclusion column (Cytiva) and eluted in NMR exchange buffer (50 mM Tris-Base pH 7.5, 50 mM KCl, 5 mM DDM, 1 mM EDTA). The tetrameric protein fractions were collected from the SEC column and concentrated to ~ 1 mg/ml for reconstitution steps.

Preparation of SSNMR samples

Lipid mixtures were prepared by combining ^{13}C-labeled PG lipids with 1-palmitoyl-2-oleoyl phosphatidyl choline (POPC or PC, Avanti Polar Lipids) to final molar ratios of 1 %, 4 %, 6 %, 8 %, 10 %, 20 %, and 30 % X_{PG} in organic solvents. The films were first dried under N_2 gas then overnight *in vacuo*. Dried films were solvated in NMR buffer (50 mM Tris-Base pH 7.5, 50 mM KCl, 1 mM EDTA) supplemented with 18.5 mM 3-[(3-cholamido-propyl)dimethylammonio]-1-propanesulfonate (CHAPS) to a final concentration of 5 mg/mL via mild sonication (cycles of 2 min on and 2 min off) with a VWR Symphony Ultrasonic Bath. Kirbac1.1 was added at 1:1 w/w ratio Lipid:Protein, corresponding to approximately 50:1 M ratio. The lipid:protein:detergent mixture was annealed for one hour at ambient temperature. Samples were diluted with NMR buffer, and detergent was subsequently removed via twice daily additions of Bio-Beads SM-2 Resin (Bio-Rad). Detergent removal was considered complete when samples became turbid, and detergent was not visible upon manual agitation. Proteoliposomes were harvested via centrifugation at 70,000 RPM for 1.5 h at 4 °C in a Ti-70 Beckman Coulter rotor. The supernatant was discarded, and the pellet resuspended in ~ 1 mL of NMR buffer for transfer. Samples were then re-pelleted using a bench-top centrifuge at 17,000 RPM for 30 min at 4 °C. Freeze-thaw cycles were performed 3–4 times with LN_2 and additional centrifugation steps to remove excess buffer. Prepared sample pellets were packed into 1.6 mm PENCIL rotors and stored ultralow until needed.

Acquisition and analysis of SSNMR data

All spectra were acquired on a 600 MHz Agilent DD2 spectrometer (Agilent Technologies, Santa Clara, CA and Loveland, CO) under Magic Angle Spinning (MAS) using a Fast-MAS 1.6 mm probe. The ^{13}C chemical shift was indirectly referenced to DSS using the downfield adamantane peak at 40.48 ppm (Morcombe and Zilm, 2003). The MAS rate was set to 12 kHz with a ^{13}C 90° pulse width of 1.4 μs and a ^{1}H 90° pulse width of 1.2 μs. 1D Direct Polarization (DP) experiments were acquired with 2048 scans and 21.6 kHz of SPINAL-64 decoupling (Fung et al., 2000) on ^{1}H. rINEPT (Elena et al., 2005) experiments were acquired with 256 scans using 1.65 ms for the first delay and 1.0 ms for the second.

1D temperature series experiments were acquired at set temperature of −50 to 20 °C in steps of 10 °C. Temperature calibration was performed as previously described (Yekefallah et al., 2024) using literature correction for radiofrequency heating under decoupling (Gottlieb et al., 1997) and sample spinning rate (Guan and Stark, 2010). The corrections resulted in a sample temperature range of −35 ± 3 to 30 ± 3 °C. 1D experiments were processed in NMRPipe (Delaglio et al., 1995) and fit using the nonlinear spectral modeling package to extrapolate peak volumes. Normalized fitting error was calculated as follows:

$$NormalizedError_i = Noise_i * \frac{\left(\frac{FittingError}{FitPeakHeight}\right)_i}{FitPeakIntensity_i} \quad (2)$$

where Fitting error:Fit Peak Height is the ratio of the nonlinear spectral modeling package fitting error calculated at each temperature 'i' used to modify the estimated spectral noise $Noise_i$, normalized to the peaks intensity.

Results and discussion

KirBac1.1 Coordinates the Physical Properties of Methylated PG Lipids

In order to investigate how KirBac1.1 orders methylated lipids in a binary lipid mixture, we first purified NA-KirBac1.1 and reconstituted into proteoliposomes with 10 % mole percentage (X_{PG}) in 90 % NA-POPC at a 1:1 protein:lipid ratio (w/w). We also generated a protein-free (PF) 10 % X_{PG} (w/w) sample in 90 % NA-POPC as a comparison to ascertain changes in the relative ratio of AT (~35 ppm) to TG (~33 ppm) in the presence and absence of KirBac1.1. The PG structure, atomic naming conventions, acyl chain identities, and ordered AT versus disordered TG acyl conformations are presented in Fig. 2A insets, as described previously (Yekefallah et al., 2024; van Aalst et al., 2022). Approximately 95 % of PG lipids are methylated at the ω-1 (Iso) or ω-2 (Anteiso) positions, identified via Gas Chromatography (van Beekveld et al., 2022). We used Direct Polarization (DP) in order to avoid biasing these results based on non-equivalent dynamics so relative changes in protein-interacting and non-interacting lipid populations could be compared. The full DP experiments for 10 % X_{PG} PF and protein-containing DP temperature series are available in the SI (Figs. S1-S2). Data was acquired at set temperatures of −50 to 20 °C, corresponding to a sample temperature range of −35 ± 3 to 30 ± 3 °C based on previously published probe calibration profile for the 1.6 mm FastMAS probe used in this work (Yekefallah et al., 2024). All subsequent references to temperature throughout the remainder of this work refer to these sample temperatures.

Temperature series excerpts are presented in Fig. 2, where spectra of 10 % X_{PG} in the presence (black) and absence (green) of KirBac1.1 at three representative temperatures are shown. Assignments are labeled on each peak. In the absence of protein at −35 ± 3 °C, AT signal (highlighted red) is observed but is overshadowed by TG signal (highlighted purple), indicating the PF sample is near the tail end of the phase transition in the absence of KirBac1.1. Of note, we previously observed this peak corresponds to two degenerate TG peaks assigned based on spatial proximity to terminal methyl groups (Yekefallah et al., 2024). While this is a relatively low transition temperature, it is not particularly

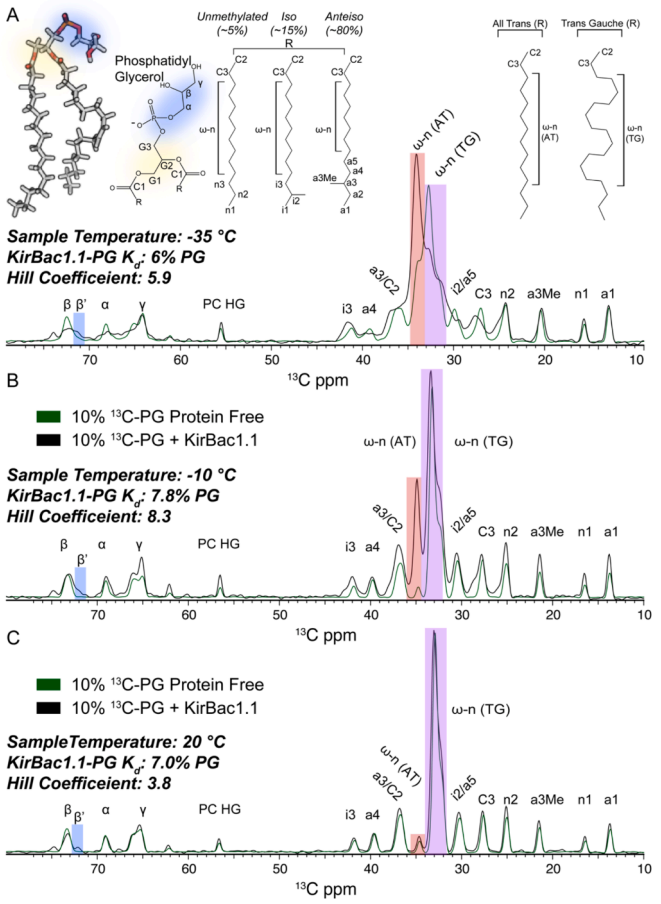

Fig. 2. Direct Polarization experiments of 10 % X_{PG} (w/w) in POPC in the presence (black) and absence (green) of KirBac1.1. (A) Structural naming convention of PG lipids used in this work, including the headgroup (left), acyl chains (middle), and conformation (right) as insets. 1D DP spectra are shown at sample temperatures of −35 °C, (B) −10 °C, and (C) 20 °C. Persistence of ordered AT signal at higher temperatures in the presence of KirBac1.1 indicates protein-driven ordering of methylated PG lipids. Spectra are presented normalized within their own temperature series since ^{13}C-PG mass per sample are nonequivalent. Protein-lipid K_d and Hill coefficients identified from previously are included (Yekefallah et al., 2024). (For interpretation of the references to colour in this figure legend, the reader is referred to the web version of this article.)

surprising giving that methylation has a strongly negative effect on lipid packing (Hirata and Axelrod, 1980), lowering melting temperature (Silvius and Mcelhaney, 1980; Lewis and McElhaney, 1985) and increasing bilayer fluiditiy (Poger et al., 2014). In the absence of protein, the phase transition was however low enough that we were not able to observe the entire transition range due to conventional spectrometer probe cooling limitations. On the other hand, AT signal is readily observed at −35 ± 3 °C when KirBac1.1 is introduced (Fig. 2A, black), and dwarfs TG signal indicating the addition of protein raises the phase transition temperature. This was a curious observation to us, since our previous work consistently found KirBac to *lower* the phase transition range. As we observe the opposite here with methylated lipids, we conclude KirBac1.1 alters transition properties to a preferred temperature range, and whether that range is increased or decreased from lipid-only samples depends on the inherent properties of the lipids themselves. As we noted before, we also observe CSPs in the headgroup region upon addition of protein. CSPs were identified as an alternate conformation of the β carbon in the PG headgroup, dubbed β', and indicate coincidence of lipid-binding and coordination of bilayer properties. This peak can be found at ~ 72 ppm and is highlighted in blue.

When the sample temperature is increased to −10 ± 3 °C, we observe that AT signal for the PF sample is nearly abolished suggesting the phase transition in the absence of protein is complete (Fig. 2B). When KirBac1.1 is introduced, the phase transition range is raised and extended such that significant AT signal is apparent. By 20 ± 3 °C the phase transition in both samples is complete (Fig. 2C). Together, this data alludes to coordination of bilayer physical properties by KirBac1.1 in the form of a raised and broadened phase transition temperature range. In our previous work, we used the NMRPipe (Delaglio et al., 1995) nonlinear spectral modeling package to fit the peak volume of β' as a function of PG concentration, at each of the temperatures presented in Fig. 2. When the results were plotted, we observed a sigmoidal shape to the data, which we fit to the Hill-Langmuir equation (equation (1) to extrapolate K_d and the Hill coefficient describing the extent of lipid-subunit cooperativity. We identified the PG-KirBac1.1 K_d to be ~ 6.0–8.0 % X_{PG} with Hill coefficients ranging from ~ 4–8, showing expected temperature-dependence of kinetics but nonetheless cooperative lipid-loading in all cases. These values are included as insets at each temperature for comparison. The data presented in Fig. 2 does however raise a number of questions: Since KirBac1.1 cooperatively binds lipids and also drives ordering, is the ordering effect also a cooperative process? Does direct lipid-protein agency play a role, and if so, is the ordering effect a byproduct of this interaction? We used exhaustive SSNMR 1D experiments to interrogate these questions throughout the remainder of this manuscript.

The extent of coordination is cooperatively dependent on PG concentration

To investigate these suppositions, we also acquired 1D DP temperature series spectra for 1 %, 4 %, 6 %, 8 %, 20 % and 30 % X_{PG}. These samples were generated at the same 1:1 w/w protein:lipid ratio, and the full DP spectra are available in the SI (Figs. S3-S8). We then fit the peaks to extrapolate peak volume for a quantitative assessment of ordering phenomena. The results of this analysis are presented in Fig. 3A, where the AT acyl conformation is presented in red and the TG population in purple. First, we consider the PF temperature series, where loss of TG signal and evolution of AT signal only just begins as the sample is cooled to below −15 °C. As PG is titrated into liposomes containing KirBac1.1, we observe increasingly more AT and less TG signal per temperature, and that the presence of AT signal as temperature is increased persists at higher temperatures. Our results indicate that KirBac1.1 raises and broadens the phase transition temperature range as suggested above. Interestingly, this phenomenon seems to be partially ameliorated above 10 % X_{PG}, where the broadening of the transition range seems to retrace. Since KirBac1.1 is saturated with PG above 10 % X_{PG} this could indicate that ordering is predicated upon protein-lipid interactions. When saturated, additional methylated lipids may unsurprisingly load into L_d domains, which will be discussed below in further detail.

Data in Fig. 3A suggests that the extent of ordering is dependent on the PG concentration in the bilayer. Since it is known that KirBac1.1's ability to order the bilayer is dependent on anionic lipid-binding to the cationic pocket (Borcik et al., 2020) and that this lipid-protein interaction is a classical Hill-type cooperative process (Yekefallah et al., 2024), would the ordering event also be a cooperative process? To investigate, we plotted the normalized AT conformation signal from each PG concentration at −35 °C, selected because all samples are approximately mid-phase transition and thus resolution between concentrations is achieved (Fig. 2B). Indeed, a sigmoidal trend between bilayer PG concentration and bilayer ordering is observed, indicating bilayer ordering is a cooperative process. Moreover, the pattern of AT signal evolution changes quite drastically at ~ 7–8 % X_{PG}, which is the same approximate concentration we previously observed to be the K_d between KirBac1.1 and methylated PG lipids (Yekefallah et al., 2024) (presented in Fig. 2, insets) when the sigmoidal bound population peak volume was fit to the Hill equation (Fig. 3C). When normalized AT signal from panel B is plotted against the corresponding protein-bound β' peak volume from

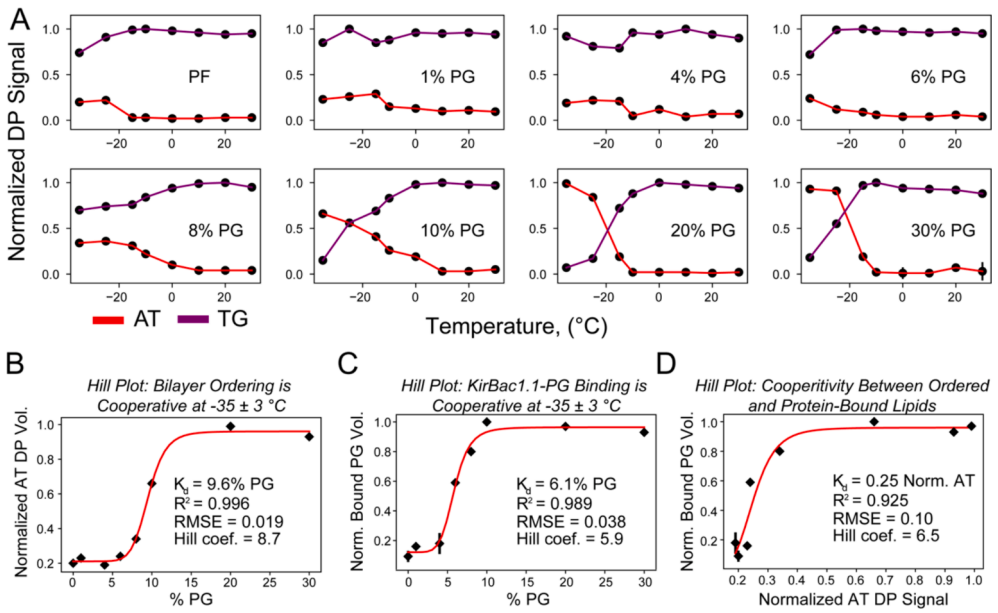

Fig. 3. The extent of ordering is dependent on PG concentration. (A) Full DP temperature series plots in the absence of KirBac1.1 (PF) and presence with 1–30 % bilayer PG content. AT (red) and TG (purple) population peak volumes are presented. (B) Hill fit of normalized AT peak volume as a function of bilayer PG showing bilayer ordering is dependent on PG concentration at −35 °C. (C) Normalized peak volume of β' from 1D DP spectra showing cooperativity between bound signal and PG concentration at −35 °C. (D) Normalized β' peak volume from (C) plotted against normalized AT peak volume from (B) showing cooperativity between lipid-binding and bilayer ordering. Error bars indicate normalized spectral noise-modified fitting error as described in the Materials and Methods. (For interpretation of the references to colour in this figure legend, the reader is referred to the web version of this article.)

panel C and Fig. 2 (blue), we observe cooperativity (Fig. 3D). This curve indicates a cooperative correlation between KirBac1.1 binding PG lipids and lipid ordering, granting further credibility to the hypothesis that KirBac1.1 surrounds itself with microdomains of ordered AT lipids by tethering anionic phospholipids via direct, long-lived protein-lipid electrostatic interactions. Furthermore, our results suggest that ordering of lipids into microdomains is predicated upon the protein-lipid interaction, which we first observed when major residues in the lipid-binding pocket shown in Fig. 1B were mutated to Gln and the ordering effect was lost (Borcik et al., 2020).

Bilayer T_m cooperatively depends on PG concentration

To reiterate the idea that lipid-binding and ordering are cooperatively dependent, we acquired refocused Insensitive Nuclei Enhanced by Polarization Transfer (rINEPT) 1D experiments to look more closely at TG population dynamics. Since rINEPT transfers magnetization through the ^{1}H–^{13}C J coupling without ^{1}H decoupling, internal dynamics are a perquisite for signal evolution (Elena et al., 2005; Alonso and Massiot, 2003; Aebischer and Ernst, 2024). Due to this, signal is not observed in the gel phase when lipids lack the requisite dynamics but will rapidly evolve upon sample heating. Evolution of the TG acyl conformation can therefore be used as a marker to accurately measure the bilayer melting temperature T_m. Since ordered AT lipid evolution is positively cooperative with lipid-binding, we hypothesized TG rINEPT signal and bound PG peak volume from DP experiments would be negatively correlated. rINEPT spectra were therefore acquired for 10 % PF as well as 4 %, 6 %, 8 %, 10 %, 20 % and 30 % X_{PG} with KirBac1.1. Full temperature series spectra are available in the SI (Figs. S9-S15).

We again observe variation in relative AT vs TG signal, as well as the pattern of TG signal evolution as a function of temperature between samples containing disparate X_{PG} concentrations (Fig. 4A). As noted above, the TG peak undergoes a slight CSP expected to be dependent on proximity to the methyl group. While this is not readily apparent from DP spectra, resolution is sufficient to distinguish in rINEPT spectra. Thus, both peaks are highlighted in purple, labeled TG, and were fit together. The full fit TG signals as a function of temperature and PG concentration are presented in Fig. 4B. It is observed that T_m increases up to 10 % X_{PG} (purple), whereby KirBac1.1 becomes saturated by PG (Yekefallah et al., 2024) (Fig. 3C). It is interesting to note that the TG melting curves retrace slightly at 20 % X_{PG} (brown), and more so at 30 % X_{PG} (pink). This observation is illustrated in the Fig. 4B inset, where the interpolated T_m from each curve is plotted. Of note, as PG concentration increases, T_m is observed to be sigmoidal indicating cooperativity between protein-lipid binding and resistance to melting until KirBac is PG-saturated. We interpret the retrace in T_m to indicate that successive additions of PG after KirBac is saturated are predominately disordered, promoting L_d domain formation and may serve to destabilize L_o formation resulting in the observed retrace in T_m. These results provide further evidence that the ordering effect is dependent on association between cationic lipid-binding pocket residues and anionic phospholipid headgroups.

We next considered TG rINEPT signal arrayed with PG concentration to understand the relationship between the two. Just as with DP spectra, we plotted normalized signal as a function of %PG and observed a sigmoidal curve (Fig. 4C). Unsurprisingly the result indicated negative cooperativity with a K_d of 6.4 % PG at −35 °C, indicating Hill-type cooperative destabilization of disorder with increased PG concentration. When TG signal at this temperature was plotted against the normalized β' peak volume from Fig. 3C, we again observe negative cooperativity. Taken together, our results provide further evidence for a cooperative relationship between KirBac1.1 binding lipids and instigating acyl ordering.

Functional connotations of supramolecular bilayer heterogeneity induced by KirBac1.1

The data presented herein paints a clear picture: when KirBac1.1 binds PG lipids, those lipids are predisposed to the ordered, AT acyl conformation despite chain methylation. Above the bilayer melting temperature, persistence of AT signal indicates formation of ordered lipid microdomains, as previously elsewhere (Borcik et al., 2020; Borcik

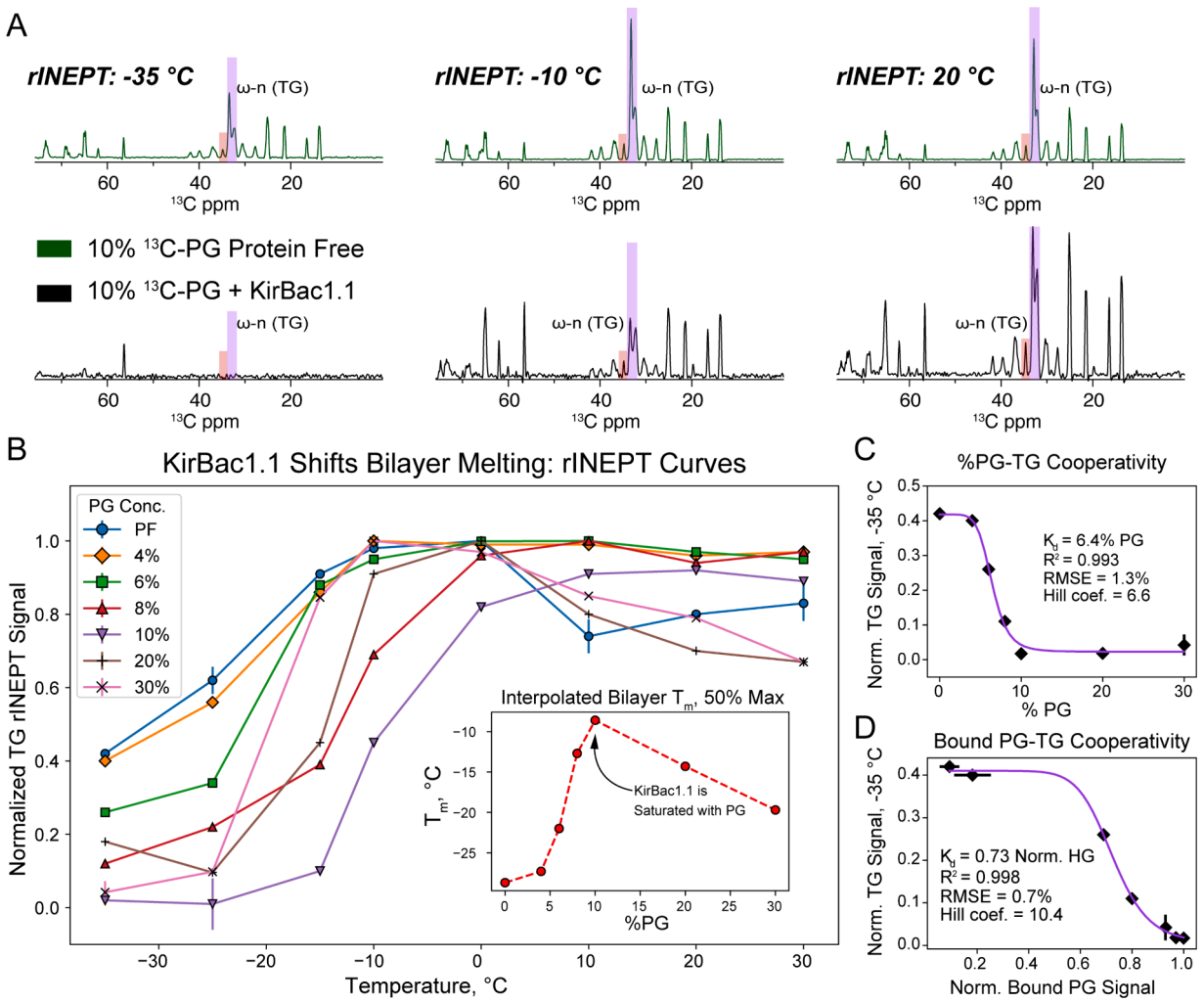

Fig. 4. Bilayer T_m Cooperatively Depends on PG Concentration. (A) Excerpts from 1D rINEPT spectra of 10 % PG in the presence (black) and absence (green) of KirBac1.1. (B) Full bilayer melting curves as a function of PG, where T_m increases with increased protein-lipid interaction until KirBac is saturated (inset). (C) Normalized TG peak volume from (B) plotted against PG concentration, identifying cooperativity between bilayer melting and successive addition of PG to the bilayer at −35 °C. (D) Normalized β' peak volume from Fig. 3C, plotted against normalized TG peak volume from (B) showing negative cooperativity between lipid-binding and bilayer melting. Error bars indicate normalized spectral noise-modified fitting error as described in the Materials and Methods. (For interpretation of the references to colour in this figure legend, the reader is referred to the web version of this article.)

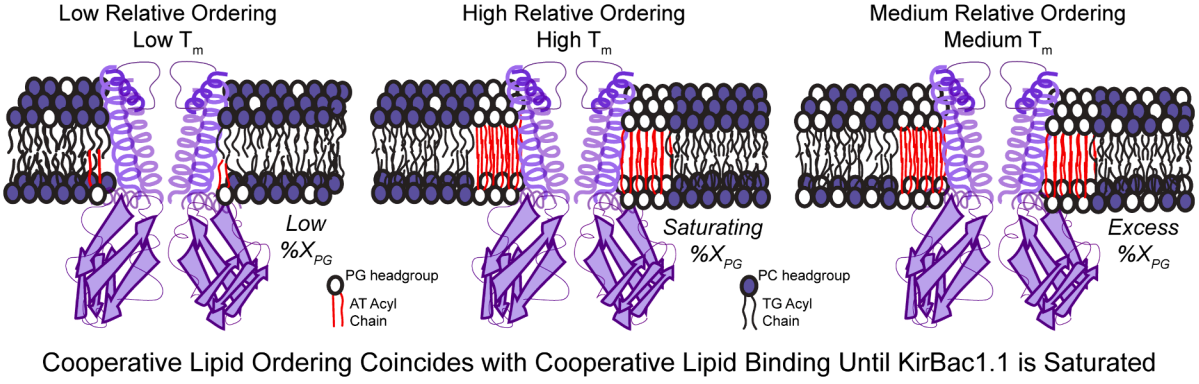

Fig. 5. Cartoon representation of how KirBac1.1 nucleates ordered domain formation. At low concentrations relative ordering, melting temperature, and levels of bound PG are low (left). As PG is titrated into the bilayer, these parameters cooperatively correlate until KirBac1.1 is saturated, characterized by high levels of relative ordering and raised melting temperatures (middle). At excess PG, additional lipids are predisposed to disordered domains, inducing decreased ordering and linearly lowering the melting temperature (right).

et al., 2019). The multiple sigmoidal correlations between AT DP signal (Fig. 3B), β' bound PG DP signal (Fig. 3C-D), and rINEPT TG signal (Fig. 4C-D) strongly suggest coaction between cooperative lipid-binding and cooperative bilayer ordering which is summarized in Fig. 5. Here, at low bilayer X_{PG} we observe correspondingly low levels of ordering, with TG signal dominating DP (Fig. 3A) and rINEPT spectra (Fig. 4B), ultimately reflected in ΔT_m (Fig. 5, left). However, upon titration of PG into the bilayer a shift occurs where AT lipids begin to dominate DP spectra at lower temperatures, the phase transition is broadened, and rINEPT signal is lost, coinciding with increasing T_m until KirBac1.1 is saturated with PG lipids. This is not a linear process: Hill-type positive sigmoidal cooperativity curves are observed between PG concentration, bound PG signal, and AT acyl signal, and negative cooperativity is observed between PG concentration, bound PG signal, and TG acyl signal. Taken together, we conclude that coordination of bilayer properties by KirBac1.1 is a cooperative process driven by protein-lipid interaction. When KirBac1.1 is saturated with PG, the bilayer is thus highly ordered manifesting as resistance to melting and a heightened T_m (Fig. 5, middle). Curiously, this trend abates shortly after, with the phase transition receding from the highest level of broadening which was observed at 10 % X_{PG} (Fig. 3A, red), return of DP TG signal at 30 % PG compared to 20 % (Fig. 3A, purple), and successive decrease in T_m extrapolated from rINEPT TG plots (Fig. 4B inset). Further, since AT DP signal and bound peak volume both plateau (Fig. 3C-D), we conclude that successive additions of lipids trend towards disorder at excess concentrations of PG. At these excess concentrations, relative ordering and T_m no longer present as strongly since a higher proportion of PG lipids are no longer protein-interacting and ordered (Fig. 5, right).

Conclusions

In our previous work we observed KirBac1.1 to nucleate ordering (Borcik et al., 2019) and that this trend could be abolished by mutation of cationic residues in the lipid binding pocket presented in Fig. 1B (Borcik et al., 2020). Here we provide additional evidence that ordered domain formation driven by KirBac1.1 is a classically Hill-type cooperative process. Interestingly, we observe strongly sigmoidal correlations between emergence of ordered SSNMR signal, disappearance of disordered signals, and evolution of bound lipid signal. Since the reciprocal AT:TG signal evolution abates simultaneously to saturation of KirBac with PG, we conclude that the ordering effect is a byproduct of direct protein lipid interaction, supported by corresponding retrace of bilayer T_m. Thus, we conclude that coordination of bilayer properties by KirBac1.1 is a cooperative process driven by protein-lipid interaction. Our results have distinct implications in our understanding of bilayer dynamics and formation of structured domains in physiological membranes. Since KirBac1.1 is highly homologous to human Kir channels, our work also poses unique ramifications for human membrane channel physiology.

Funding

This work was funded by NIH grant R35GM124979 (Maximizing Investigators' Research Award [MIRA] R35) to B.J.W. This project has also received funding from the European Union's Horizon Europe grant and innovation program under grant agreement no. 101,045,485 to M. W.

CRediT authorship contribution statement

Evan J. van Aalst: . **Maryam Yekefallah:** Conceptualization, Data curation, Formal analysis, Investigation, Methodology, Visualization. **Roy A. M. van Beekveld:** . **Eefjan Breukink:** Conceptualization, Methodology. **Markus Weingarth:** Conceptualization, Funding acquisition, Investigation, Methodology, Project administration, Writing – original draft. **Benjamin J. Wylie:** Conceptualization, Data curation, Formal analysis, Funding acquisition, Investigation, Methodology, Project administration, Resources, Supervision, Validation, Visualization, Writing – original draft, Writing – review & editing.

Declaration of competing interest

The authors declare that they have no known competing financial interests or personal relationships that could have appeared to influence the work reported in this paper.

Data availability

Data will be made available on request.

Appendix A. Supplementary data

Supplementary data to this article can be found online at https://doi.org/10.1016/j.yjsbx.2024.100101.

References

Aebischer, K., Ernst, M., 2024. INEPT and CP transfer efficiencies of dynamic systems in MAS solid-state NMR. J. Magn. Reson. 359, 107617 https://doi.org/10.1016/j.jmr.2024.107617.

Ahuja, S., Hornak, V., Yan, E.C., Syrett, N., Goncalves, J.A., Hirshfeld, A., Ziliox, M., Sakmar, T.P., Sheves, M., Reeves, P.J., et al., 2009. Helix movement is coupled to displacement of the second extracellular loop in rhodopsin activation. Nat. Struct. Mol. Biol. 16, 168–175. https://doi.org/10.1038/nsmb.1549.

Alonso, B., Massiot, D., 2003. Multi-scale NMR characterisation of mesostructured materials using 1H–>13C through-bond polarisation transfer, fast MAS, and 1H spin diffusion. J. Magn. Reson. 163, 347–352. https://doi.org/10.1016/s1090-7807(03)00061-2.

Amani, R., Borcik, C., Khan, N., Versteeg, D., Yekefallah, M., Do, H., Coats, H., Wylie, B., 2020. Conformational changes upon gating of KirBac1.1 into an open-activated state revealed by solid-state NMR and functional assays. PNAS 117, 2938–2947. https://doi.org/10.1073/pnas.1915010117.

Amani, R., Schwieters, C.D., Borcik, C.G., Eason, I.R., Han, R., Harding, B.D., Wylie, B.J., 2021. Water Accessibility Refinement of the Extended Structure of KirBac1.1 in the Closed State. Front. Mol. Biosci. 8, 772855 https://doi.org/10.3389/fmolb.2021.772855.

Baccouch, R., Rascol, E., Stoklosa, K., and Alves, I.D. (2022). The role of the lipid environment in the activity of G protein coupled receptors.

Becker-Baldus, J., Yeliseev, A., Joseph, T.T., Sigurdsson, S.T., Zoubak, L., Hines, K., Iyer, M.R., van den Berg, A., Stepnowski, S., Zmuda, J., et al., 2023. Probing the Conformational Space of the Cannabinoid Receptor 2 and a Systematic Investigation of DNP-Enhanced MAS NMR Spectroscopy of Proteins in Detergent Micelles. ACS Omega 8, 32963–32976. https://doi.org/10.1021/acsomega.3c04681.

Belin, B., Busset, N., Giraud, E., Molinaro, A., Silipo, A., Newman, D., 2018. Hopanoid lipids: from membranes to plant-bacteria interactions. Nat. Rev. Microbiol. 16, 304–315. https://doi.org/10.1038/nrmicro.2017.173.

Bligh, E., Dyer, W., 1959. A Rapid Method of Total Lipid Extraction and Purification. Can. J. Biochem. Physiol. 37, 911–917.

Borcik, C.G., Versteeg, D.B., Wylie, B.J., 2019. An Inward-Rectifier Potassium Channel Coordinates the Properties of Biologically Derived Membranes. Biophys. J . https://doi.org/10.1016/j.bpj.2019.03.023.

Borcik, C.G., Versteeg, D.B., Amani, R., Yekefallah, M., Khan, N.H., Wylie, B.J., 2020. The Lipid Activation Mechanism of a Transmembrane Potassium Channel. J. Am. Chem. Soc. 142, 14102–14116. https://doi.org/10.1021/jacs.0c01991.

Borcik, C.G., Eason, I.R., Vanderloop, B., Wylie, B.J., 2022. 2H,13C-Cholesterol for Dynamics and Structural Studies of Biological Membranes. American Chemical Society.

Borcik, C.G., Eason, I.R., Yekefellah, M., Amani, R., Han, R., Vanderloop, B.H., Wylie, B., 2022. A Cholesterol Dimer Stabilizes the Inactivated State of an Inward-rectifier Potassium Channel. Angew. Chem. Int. Ed. Engl. 61, e202112232.

Brown, D., London, E., 1998. Structure and origin of ordered lipid domains in biological membranes. J. Membr. Biol. 164, 103–114. https://doi.org/10.1007/s002329900397.

Brown, D., London, E., 1998. Functions of lipid rafts in biological membranes. Annu. Rev. Cell Dev. Biol. 14, 111–136. https://doi.org/10.1146/annurev.cellbio.14.1.111.

Calmet, P., Cullin, C., Cortes, S., Vang, M., Caudy, N., Baccouch, R., Dessolin, J., Maamar, N.T., Lecomte, S., Tillier, B., Alves, I.D., 2020. Cholesterol impacts chemokine CCR5 receptor ligand-binding activity. FEBS J. 287, 2367–2385. https://doi.org/10.1111/febs.15145.

Cheng, W.W.L., Enkvetchakul, D., Nichols, C.G., 2009. KirBac1.1: it's an inward rectifying potassium channel. J. Gen. Physiol. 133, 295–305. https://doi.org/10.1085/jgp.200810125.

Clarke, O., Caputo, A., Hill, A., Vandenberg, J., Smith, B., Gulbis, J., 2010. Domain reorientation and rotation of an intracellular assembly regulate conduction in Kir

potassium channels. Cell 141, 1018–1029. https://doi.org/10.1016/j.cell.2010.05.003.
D'Avanzo, N., Cheng, W.W.L., Doyle, D.A., Nichols, C.G., 2010. Direct and Specific Activation of Human Inward Rectifier K+ Channels by Membrane Phosphatidylinositol 4,5-Bisphosphate. J. Biol. Chem. 285, 37129–37132. https://doi.org/10.1074/jbc.C110.186692.
Delaglio, F., Frzesiek, S., Vuister, G., Zhu, G., Pfeifer, J., Bax, A., 1995. NMRPipe- A multidimensinoal spectral processing system based on Unix Pipes. J. Biomol. NMR 6, 277–293. https://doi.org/10.1007/BF00197809.
Della Ripa, L.A., Courtney, J.M., Phinney, S.M., Borcik, C.G., Burke, M.D., Rienstra, C.M., Pogorelov, T.V., 2023. Segmental Dynamics of Membranous Cholesterol are Coupled. J. Am. Chem. Soc. 145, 15043–15048. https://doi.org/10.1021/jacs.3c01775.
Elena, B., Lesage, A., Steuernagel, S., Böckmann, A., Emsley, L., 2005. Proton to carbon-13 INEPT in solid-state NMR spectroscopy. J. Am. Chem. Soc. 127, 17296–17302. https://doi.org/10.1021/ja054411x.
Fung, B., Khitrin, A., Ermolaev, K., 2000. An improved broadband decoupling sequence for liquid crystals and solids. J. Magn. Reson. 142, 97–101. https://doi.org/10.1006/jmre.1999.1896.
Gottlieb, H.E., Kotlyar, V., Nudelman, A., 1997. NMR Chemical Shifts of Common Laboratory Solvents as Trace Impurities. J. Org. Chem. 62, 7512–7515. https://doi.org/10.1021/jo971176v.
Guan, X., Stark, R.E., 2010. A general protocol for temperature calibration of MAS NMR probes at arbitrary spinning speeds. Solid State Nucl. Magn. Reson. 38, 74–76. https://doi.org/10.1016/j.ssnmr.2010.10.001.
Hansen, S.B., Tao, X., MacKinnon, R., 2011. Structural basis of PIP2 activation of the classical inward rectifier K+ channel Kir2.2. Nature 477, 495–U152. https://doi.org/10.1038/nature10370.
Hibino, H., Inanobe, A., Furutani, K., Murakami, S., Findlay, I., Kurachi, Y., 2010. Inwardly rectifying potassium channels: their structure, function, and physiological roles. Physiol. Rev. 90, 291–366. https://doi.org/10.1152/physrev.00021.2009.
Hill, A.V., 1909. The mode of action of nicotine and curari, determined by the form of the contraction curve and the method of temperature coefficients. J. Physiol. 39, 361–373. https://doi.org/10.1113/jphysiol.1909.sp001344.
Hill, A.V., 1913. The Combinations of Haemoglobin with Oxygen and with Carbon Monoxide. I. Biochem J 7, 471–480. https://doi.org/10.1042/bj0070471.
Hirata, F., Axelrod, J., 1980. PHOSPHOLIPID METHYLATION AND BIOLOGICAL SIGNAL TRANSMISSION. Science 209, 1082–1090. https://doi.org/10.1126/science.6157192.
Huang, C., Feng, S., Hilgemann, D., 1998. Direct activation of inward rectifier potassium channels by PIP2 and its stabilization by G beta gamma. Nature 391, 803–806. https://doi.org/10.1038/35882.
Kimata, N., Pope, A., Eilers, M., Opefi, C.A., Ziliox, M., Hirshfeld, A., Zaitseva, E., Vogel, R., Sheves, M., Reeves, P.J., Smith, S.O., 2016. Retinal orientation and interactions in rhodopsin reveal a two-stage trigger mechanism for activation. Nat. Commun. 7, 12683. https://doi.org/10.1038/ncomms12683.
Kimata, N., Pope, A., Sanchez-Reyes, O.B., Eilers, M., Opefi, C.A., Ziliox, M., Reeves, P.J., Smith, S.O., 2016. Free backbone carbonyls mediate rhodopsin activation. Nat. Struct. Mol. Biol. 23, 738–743. https://doi.org/10.1038/nsmb.3257.
Kwon, B., Waring, A., Hong, M., 2013. A H-2 solid-state NMR study of lipid clustering by cationic antimicrobial and cell-penetrating peptides in model bacterial membranes. Biophys. J . 105, 2333–2342. https://doi.org/10.1016/j.bpj.2013.08.020.
Laganowsky, A., Reading, E., Allison, T.M., Ulmschneider, M.B., Degiacomi, M.T., Baldwin, A.J., Robinson, C.V., 2014. Membrane proteins bind lipids selectively to modulate their structure and function. Nature 510, 172–175. https://doi.org/10.1038/nature13419.
Langmuir, I., 1918. THE ADSORPTION OF GASES ON PLANE SURFACES OF GLASS, MICA AND PLATINUM. J. Am. Chem. Soc. 40, 1361–1403. https://doi.org/10.1021/ja02242a004.
Lewis, R.N., McElhaney, R.N., 1985. Thermotropic phase behavior of model membranes composed of phosphatidylcholines containing iso-branched fatty acids. 1. Differential Scanning Calorimetric Studies. Biochemistry 24, 2431–2439. https://doi.org/10.1021/bi00331a007.
Lopatin, A.N., Makhina, E.N., Nichols, C.G., 1994. Potassium channel block by cytoplasmic polyamines as the mechanism of intrinsic rectification. Nature 372, 366–369. https://doi.org/10.1038/372366a0.
Matamoros, M., and Nichols, C. (2021). Pore-forming transmembrane domains control ion selectivity and selectivity filter conformation in the KirBac1.1 potassium channel. J Gen Physiol *153*, ARTN e202012683. 10.1085/jgp.202012683.
Meng, X.Y., Zhang, H.X., Logothetis, D.E., Cui, M., 2012. The molecular mechanism by which PIP(2) opens the intracellular G-loop gate of a Kir3.1 channel. Biophys. J . 102, 2049–2059. https://doi.org/10.1016/j.bpj.2012.03.050.
Mertz, B., Struts, A.V., Feller, S.E., Brown, M.F., 2012. Molecular simulations and solid-state NMR investigate dynamical structure in rhodopsin activation. Biochim. Biophys. Acta 1818, 241–251. https://doi.org/10.1016/j.bbamem.2011.08.003.
Mitchison-Field, L.M., Belin, B.J., 2023. Bacterial lipid biophysics and membrane organization. Curr. Opin. Microbiol. 74, 102315 https://doi.org/10.1016/j.mib.2023.102315.
Morcombe, C., Zilm, K., 2003. Chemical shift referencing in MAS solid state NMR. J. Magn. Reson. 162, 479–486. https://doi.org/10.1016/S1090-7807(03)00082-X.
Morvan, E., Taib-Maamar, N., Grélard, A., Loquet, A., Dufourc, E.J., 2023. Biomembranes: Picosecond to second dynamics and plasticity as deciphered by solid state NMR. Biochim. Biophys. Acta Biomembr. 1865, 184097 https://doi.org/10.1016/j.bbamem.2022.184097.
Morvan, E., Taib-Maamar, N., Grélard, A., Loquet, A., Dufourc, E.J., 2023. Dynamic Sorting of Mobile and Rigid Molecules in Biomembranes by Magic-Angle Spinning. Anal. Chem. 95, 3596–3605. https://doi.org/10.1021/acs.analchem.2c04185.
Patrick, J.W., Boone, C.D., Liu, W., Conover, G.M., Liu, Y., Cong, X., Laganowsky, A., 2018. Allostery revealed within lipid binding events to membrane proteins. PNAS 115, 2976–2981. https://doi.org/10.1073/pnas.1719813115.
Poger, D., Caron, B., Mark, A.E., 2014. Effect of methyl-branched fatty acids on the structure of lipid bilayers. J. Phys. Chem. B 118, 13838–13848. https://doi.org/10.1021/jp503910r.
Purusottam, R., Senicourt, L., Lacapere, J., Tekely, P., 2015. Probing the gel to liquid-crystalline phase transition and relevant conformation changes in liposomes by C-13 magic-angle spinning NMR spectroscopy. BBA-Biomembranes 1848, 3134–3139. https://doi.org/10.1016/j.bbamem.2015.09.011.
Ray, A.P., Thakur, N., Pour, N.G., Eddy, M.T., 2023. Dual mechanisms of cholesterol-GPCR interactions that depend on membrane phospholipid composition. Structure. https://doi.org/10.1016/j.str.2023.05.001.
Schneider, M., Marsh, D., Jahn, W., Kloesgen, B., and Heimburg, T. (1999). Network formation of lipid membranes: Triggering structural transitions by chain melting. Proceedings of the National Academy of Sciences of the United States of America *96*, 14312-14317. 10.1073/pnas.96.25.14312.
Sefah, E., Mertz, B., 2021. Bacterial Analogs to Cholesterol Affect Dimerization of Proteorhodopsin and Modulates Preferred Dimer Interface. J. Chem. Theory Comput. 17, 2502–2512. https://doi.org/10.1021/acs.jctc.0c01174.
Silvius, J.R., Mcelhaney, R.N., 1980. Effects of Phospholipid Acyl Chain Structure on Thermotropic Phase Properties. 3. Phosphatidylcholines with (-)-Anteiso and (+/-)-Anteiso Acyl Chains. Chem. Phys. Lipids 26, 67–77.
Soom, M., Schonherr, R., Kubo, Y., Kirsch, C., Klinger, R., Heinemann, S., 2001. Multiple PIP2 binding sites in Kir-2.1 inwardly rectifying potassium channels. FEBS Lett. 490, 49–53. https://doi.org/10.1016/S0014-5793(01)02136-6.
Thakur, N., Ray, A.P., Sharp, L., Jin, B., Duong, A., Pour, N.G., Obeng, S., Wijesekara, A. V., Gao, Z.G., McCurdy, C.R., et al., 2023. Anionic phospholipids control mechanisms of GPCR-G protein recognition. Nat. Commun. 14, 794. https://doi.org/10.1038/s41467-023-36425-z.
van Aalst, E.J., Borcik, C.G., Wylie, B.J., 2022. Spectroscopic signatures of bilayer ordering in native biological membranes. Biochim. Biophys. Acta Biomembr. 1864, 183891 https://doi.org/10.1016/j.bbamem.2022.183891.
van Aalst, E.J., McDonald, C.J., Wylie, B.J., 2023. Cholesterol Biases the Conformational Landscape of the Chemokine Receptor CCR3: A MAS SSNMR-Filtered Molecular Dynamics Study. J. Chem. Inf. Model. 63, 3068–3085. https://doi.org/10.1021/acs.jcim.2c01546.
van Aalst, E.J., Wylie, B.J., 2021. Cholesterol is a Dose-Dependent Positive Allosteric Modulator of CCR3 Ligand Affinity and G Protein Coupling. Front. Mol. Biosci. 8, 718. https://doi.org/10.3389/fmolb.2021.724603.
van Beekveld, R.A.M., Derks, M.G.N., Kumar, R., Smid, L., Maass, T., Medeiros-Silva, J., Breukink, E., Weingarth, M., 2022. Specific Lipid Studies in Complex Membranes by Solid-State NMR Spectroscopy. Chemistry 28, e202202472.
Vist, M.R., Davis, J.H., 1990. Phase equilibria of cholesterol/dipalmitoylphosphatidylcholine mixtures: 2H nuclear magnetic resonance and differential scanning calorimetry. Biochemistry 29, 451–464. https://doi.org/10.1021/bi00454a021.
Wang, S.Z., Alimi, Y., Tong, A., Nichols, C.G., Enkvetchakul, D., 2009. Stabilization of KirBac1.1 Tetramer by Blocking Ions. Biophys. J . 96, 467a–a.
Warnet, X., Laadhari, M., Arnold, A., Marcotte, I., Warschawski, D., 2016. A H-2 magic-angle spinning solid-state NMR characterisation of lipid membranes in intact bacteria. BBA-Biomembranes 1858, 146–152. https://doi.org/10.1016/j.bbamem.2015.10.020.
Whorton, M.R., MacKinnon, R., 2011. Crystal structure of the mammalian GIRK2 K+ channel and gating regulation by G proteins, PIP2, and sodium. Cell 147, 199–208. https://doi.org/10.1016/j.cell.2011.07.046.
Xie, L., John, S., Ribalet, B., Weiss, J., 2008. Phosphatidylinositol-4,5-bisphosphate (PIP (2)) regulation of strong inward rectifier Kir2.1 channels: multilevel positive cooperativity. Journal of Physiology-London 586, 1833–1848. https://doi.org/10.1113/jphysiol.2007.147868.
Yekefallah, M., Rasberry, C.A., van Aalst, E.J., Browning, H.P., Amani, R., Versteeg, D.B., Wylie, B.J., 2022. Mutational Insight into Allosteric Regulation of Kir Channel Activity. ACS Omega 7, 43621–43634. https://doi.org/10.1021/acsomega.2c04456.
Yekefallah, M., van Aalst, E., van Beekveld, R., Eason, I., Breukink, E., Weingarth, M., Wylie, B., 2024. Cooperative Gating of a K+ Channel by Unmodified Biological Anionic Lipids Viewed by Solid-State NMR Spectroscopy. J. Am. Chem. Soc.